Extent Estimation of Sailing Boats Applying Elliptic Cones to 3D LiDAR Data

Tim Baur and Johannes Reuter
Institute of System Dynamics (ISD)
University of Applied Sciences Konstanz (HTWG)
Konstanz, Germany
{tbaur,jreuter}@htwg-konstanz.de

Antonio Zea and Uwe D. Hanebeck
Intelligent Sensor-Actuator-Systems Laboratory (ISAS)
Karlsruhe Institute of Technology (KIT)
Karlsruhe, Germany
{antonio.zea,uwe.hanebeck}@kit.edu

***Abstract*—In this paper, approximating the shape of a sailing boat using elliptic cones is investigated. Measurements are assumed to be gathered from the target's surface recorded by 3D scanning devices such as multilayer LiDAR sensors. Therefore, different models for estimating the sailing boat's extent are presented and evaluated in simulated and real-world scenarios. In particular, the measurement source association problem is addressed in the models. Simulated investigations are conducted with a static and a moving elliptic cone. The real-world scenario was recorded with a Velodyne Alpha Prime (VLP-128) mounted on a ferry of Lake Constance. Final results of this paper constitute the extent estimation of a single sailing boat using LiDAR data applying various measurement models.**

***Index Terms*—3D Extended Object Tracking (EOT), Sailing Boat, Elliptic Cone, LiDAR.**

I. Introduction

As the resolution and accuracy of modern sensors increase, more and more information can be extracted out of recorded environment data. In earlier perception systems, sensors merely gathered a single measurement per target and time step, which resulted in modeling the targets as mathematical points. Nowadays, multiple measurements per time step from a single target are common. Processing all these measurements enables estimating the target's extent [1] instead of tracking the targets as a single point.

In recent years, numerous articles have been published examining the extension estimation of dynamic objects applying various 2D sensor data. Thus, models assuming elliptical [2]–[5] or rectangular shapes [6]–[8] have been proposed to estimate the extent of different objects. These models fit well for a great majority of targets in 2D space such as ellipses for pedestrians, cyclists, or ships in maritime applications and rectangles for cars in automotive applications. Moreover, if prior knowledge of the types of occurring targets is available, learned spatial distribution models applying variational Gaussian mixture models [9]–[11] can be utilized. If no prior knowledge about the target's extent or shape is available and measurement sources on the target are modeled accurately, inference about the target's shape itself can be performed. This can be achieved by modeling the shape as star-convex radial function represented using a Fourier series expansion [12] or a Gaussian process [13], [14].

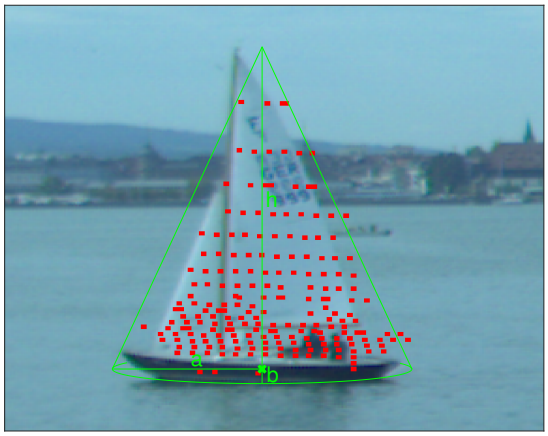

Fig. 1: 3D LiDAR measurements of sailing boat and elliptic cone as shape approximation.

However, modern devices such as multilayer LiDAR sensors or depth cameras gather the environment in 3D instead of 2D space. Thus, measurement models processing this data should be defined in 3D space as well. Models such as in [2], [3] can be generalized to estimate the target's extent by means of ellipsoids. Moreover, basic geometric shapes such as cylinders can be applied in modified random hypersurface models (RHMs) [15]–[17] where extrusions are modeled using a spatial distribution. As in 2D space, shapes can be estimated in 3D space if no prior knowledge of the shape or the extent is available and measurement sources on the outer hull of the target are modeled accurately. This can be achieved by representing the target's shape as star-convex radial function in spherical coordinates expanded by spherical harmonics [18], spherical double Fourier series [19] or Gaussian processes [20]. When tracking targets in 3D space, applied models should match the application in terms of complexity so that the most efficient method is used. If the shape information of the target is desired or highly accurate estimates of the system are needed, a shape estimation procedure is more suitable. Otherwise, shape approximation algorithms are way more efficient in terms of computational effort as the fixed shapes can be represented with much fewer parameters.

The contribution of this paper is to propose two models for

the extent estimation of sailing boats. In maritime applications, ships can be assumed to have an elliptical shape [21] when estimated in 2D space. However, when 3D measurements of multilayer LiDAR sensors are processed, applying an ellipsoidal shape for every class of maritime objects is not sufficient. In Fig. 1, measurements of a sailing boat can be seen. The measurements were recorded by a ferry on Lake Constance, which had to pass through a regatta. It is clearly evident that an ellipsoidal shape is not appropriate for this class of maritime objects. Therefore, the contribution of this paper is to apply cones with an elliptical base as shape approximation for sailing boats in 3D space. The objective is to estimate the extent of the boat by means of length a, width b, and height h, as can be seen in Fig.1. For this purpose, different models for the estimation of a cone shape with an elliptical base are presented in this paper and evaluated using simulations and real data.

The remainder of this paper is structured as follows. First, in Sec. II details on the problem formulation and further basics are given. In Sec. III, different measurement models for estimating an elliptic cone are presented. Thus, a greedy measurement association model (GAM) and an extrusion RHM with a GAM component [16] are presented. In Sec. IV, implementation methods for the different models are presented. In this paper, the models are implemented using a smart sampling Kalman filter (S²KF) [22] for all measurement association techniques presented in Sec. III. Afterwards, the models are investigated in Monte Carlo simulations with static and dynamic objects in Sec. V and in a real-world scenario for a single sailing boat in Sec. VI. The paper ends with the conclusion and proposals for future work in Sec. VII.

II. Fundamentals

In this section, details on expected measurements and the system state are given. Furthermore, particulars on the assumed shape and on modeling extended objects in 3D space are specified.

A. Measurements and likelihood

In this paper, a measurement set with n_k measurements $\mathcal{Y}_k = \left\{\underline{y}_{k,l}\right\}_{l=1}^{n_k}$ of the target's boundary is assumed to be recorded at every time step k. Each measurement is given in 3D Cartesian space $\underline{y}_{k,l} \in \mathbb{R}^3$. As measurements are assumed to be mutually independent, the likelihood can be expressed as

$$p\left(\mathcal{Y}_k|\underline{x}_k\right) = \prod_{l=1}^{n_k} p\left(\underline{y}_{k,l}|\underline{x}_k\right) \tag{1}$$

with state variable $\underline{x}_k$. Thus, it is sufficient to specify the measurement model and the measurement likelihood for a single measurement. The likelihood encodes the probability of a single measurement being recorded given a specific system state. Finally, the state distribution $p(\underline{x}_k)$ can be estimated using recorded measurements and the likelihood by applying Bayes' rule. Please note that indices k, l will be omitted if not needed as the measurement model and the likelihood will be developed for a single measurement at a single time step.

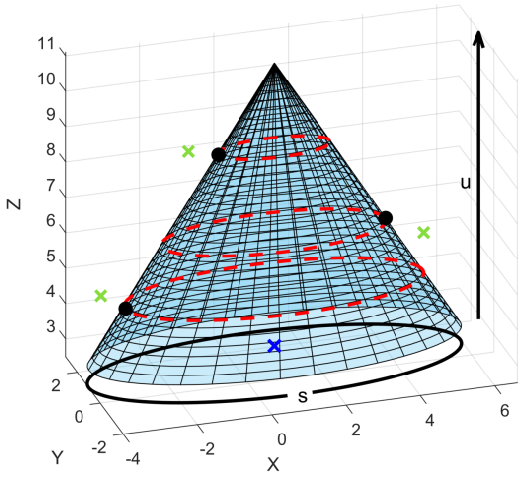

Fig. 2: Illustration of an elliptic cone. Position as blue cross, measurements as green crosses, measurement sources as black balls and slices as red dashed ellipses.

B. System state

The system state comprises the position $\underline{m}_k$, orientation ψ_k, velocity components $\underline{v}_k$ and the shape parameters $\underline{p}_k$ and is given as

$$\underline{x}_k = \left[\underline{m}_k^T, \psi_k, \underline{v}_k^T, \underline{p}_k^T\right]^T. \tag{2}$$

Please note that in this paper, we limit ψ_k to the orientation of the target in the xy-plane, namely the yaw angle. However, also all three rotation angles in Euler angles or quaternions as described in [20] could be used to describe the orientation of the target in 3D space. In dynamic scenarios, objects are assumed to evolve with a coordinated turn model [23] over time in this paper.

C. Elliptic cone

The shape investigated in this work is an elliptic cone as an approximation for sailing boats in 3D space. An elliptic cone can be represented in parametric form as [16]

$$c(u, s, \underline{p}) = \begin{bmatrix} (1-u)\cdot a \cdot \cos(s) \\ (1-u)\cdot b \cdot \sin(s) \\ u \cdot h \end{bmatrix}, \tag{3}$$

with major half axis a and minor half axis b of the base ellipse and height h. Thus, the shape parameters are given as $\underline{p}_k = [a_k, b_k, h_k]^T$. Please note that $\underline{p}$ as function argument highlights the dependence on the actual shape parameters. The parameter $u \in [0, 1]$ is used to linearly scale the base ellipse with the full ellipse at the bottom and a single point at the top. The parameter $s \in [0, 2\pi]$ lets us iterate through all points on a specific height. An ellipse on a specific height in parallel to the xy-plane will be called *slice* in the further course of this paper. An illustration of an elliptic cone and the defining parameters can be seen in Fig. 2. The position of the elliptic cone is located in the center of the base ellipse.

D. Modeling 3D extended objects

The measurement is assumed to be generated based on a measurement source model given as

$$\begin{aligned}\underline{y} &= \underline{z} + \underline{w} \\ &= c(u, s, \underline{p}) + \underline{w}\end{aligned} \tag{4}$$

with measurement source $\underline{z}$. We assume Gaussian noise $\underline{w} \sim \mathcal{N}(\underline{0}, \mathbf{C}_w)$ in this paper so we can apply Gaussian sampling techniques [22]. The likelihood depends on the parameters u and s and can be given as the marginal distribution [16]

$$p(\underline{y}|\underline{x}) = \int_U \int_S p(\underline{y}|\underline{x}, s, u) \cdot p(s, u|\underline{x})\, ds\, du. \tag{5}$$

Both parts of this likelihood can be interpreted differently. The likelihood $p(\underline{y}|\underline{x}, s, u)$ can be regarded as the sensor model, which is defined through the noise density $f_W(\underline{w})$. The distribution $p(s, u|\underline{x})$ expresses the source model. Since the actual source of a specific measurement is unknown, we have to deal with the well-known *measurement source association problem* [24]. An illustration of the association problem can be seen in Fig. 2, where measurements and measurement sources on a specific slice are depicted. In the remainder of this work we will present various approaches for solving this association problem. As the parameters u and s will be modeled differently in the RHM with GAM component, the likelihood (5) is finally split up as

$$p(\underline{y}|\underline{x}) = \int_U \int_S p(\underline{y}|\underline{x}, s, u) \cdot p(s|\underline{x}, u) \cdot p(u|\underline{x})\, ds\, du \tag{6}$$

using the approximation $p(s, u|\underline{x}) = p(s|\underline{x}, u) \cdot p(u|\underline{x})$ [25, pp. 79], [16]. In the following, both likelihoods (5) and (6) will be used to develop different approaches to deal with the association problem.

III. Measurement Models

Based on Sec. II-D, we want to present two different measurement models to estimate the extent of a sailing boat modeled by an elliptic cone. The presentation of these models is arranged in ascending order by means of robustness, effectiveness, and accuracy. Some difficulties of the models are also addressed. Implementations for every model will be given in Sec. IV.

A. Spatial distribution model (SDM)

For completeness, SDMs are briefly addressed in this section, but not implemented in this work. A well-known example of SDMs are random matrices [2]. However, many other approaches to model extended targets using a spatial distribution exist. In the likelihood (5), the development of an SDM would mean that the distribution $p(s, u|\underline{x})$ has to be modeled explicitly. Thus, a common approach is to assume measurements to be recorded uniformly distributed from the whole surface. It is well known that SDMs yield unbiased estimates even in the presence of high noise [16]. However, this is only the case if the measurements actually fit the assumed distribution. Otherwise, the estimate may be biased. In the presence of partial occlusions and different viewing angles, constructing a proper spatial distribution would be very difficult, computationally expensive, and is therefore neglected in this paper.

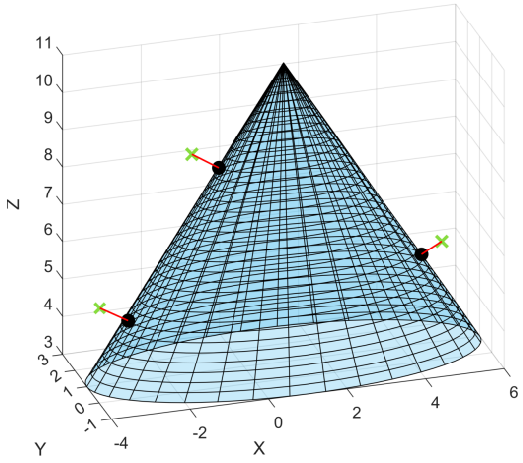

Fig. 3: Illustration of GAM with red distance lines being perpendicular to the surface.

B. Greedy association model (GAM)

A GAM [25, pp. 29–32] [24] is an intuitive but also naive approach of solving the association problem for extended objects. Here, the measurement source on the surface of the shape is assumed to be the most likely one, or, in our case, the point on the surface with the smallest distance $c(\hat{u}, \hat{s}, \underline{p})$ to the actual measurement. Thus, the mass of the source model $p(s, u|\underline{x})$ is reduced to the Dirac δ-distribution

$$p(s, u|\underline{x}) = \delta\left(s - \hat{s}, u - \hat{u}\right). \tag{7}$$

Therefore, the likelihood (5) is reduced to a Gaussian distribution around the most likely point defined by the measurement noise given as

$$p(\underline{y}|\underline{x}) = \mathcal{N}\left(\underline{y}; c(\hat{u}, \hat{s}, \underline{p}), \mathbf{C}_w\right). \tag{8}$$

An illustration of a GAM is depicted in Fig. 3 where each measurement is allocated to a specific point on the surface. The point on the surface of an elliptic cone with the smallest distance to the measurement $\underline{\tilde{y}} = [\tilde{y}_x, \tilde{y}_y, \tilde{y}_z]^T$ can be calculated as the intersection of a normal through the measurement with the surface. The parameter $\hat{s}$ can be calculated as

$$\begin{aligned}\hat{s} &= \cos^{-1}\left(\frac{a\,\tilde{y}_x}{(1-\hat{u})\,a^2 - \hat{u}\,h^2 - \tilde{y}_z\,h}\right) \\ &= \sin^{-1}\left(\frac{b\,\tilde{y}_y}{(1-\hat{u})\,b^2 - \hat{u}\,h^2 - \tilde{y}_z\,h}\right)\end{aligned} \tag{9}$$

with given parameter $\hat{u}$. Using the equality $\sin\left(\cos^{-1}(x)\right) = \sqrt{1-x^2}$, the quartic equation

$$1 - \frac{\tilde{y}_x^2\, a^2}{\left((1-\hat{u})\, a^2 - \hat{u}\, h^2 - \tilde{y}_z\, h\right)^2} = \frac{\tilde{y}_y^2\, b^2}{\left((1-\hat{u})\, b^2 - \hat{u}\, h^2 - \tilde{y}_z\, h\right)^2} \tag{10}$$

results, which can be solved using a symbolic math software. Please note, that $\underline{\tilde{y}}$ is the measurement $\underline{y}$ in local coordinates. GAMs are known to be biased in the presence of high noise [24] and additionally not capable of robustly estimating length or height parameters [25, pp. 74–79]. However, the model can still produce adequate estimates and is the most basic approach of solving the association problem.

C. Extrusion RHM

Another way of solving the association problem is given in this section by redefining a basic tool of extended object tracking (EOT), namely RHMs [3], [16], [17]. When using RHMs, fundamental tools of EOT are combined in a single model. In this case, an RHM consists of the combination of an SDM and a GAM. When using 2D RHMs [3], [12], the measurement source at the border of a closed shape is modeled using a GAM. Additionally, measurements of the shape's interior are represented using a scaling factor $s \in [0, 1]$, which is modeled as actual 1D distribution. This formulation can be used for modeling 3D measurement models by adapting the likelihood (6) [15]–[17]. Therefore, the distribution $p(s|\underline{x}, u)$ is modeled as Dirac δ-distribution

$$p(s|\underline{x}, u) = \delta(s - \hat{s}) \tag{11}$$

and hence as GAM for a given slice u. The slice distribution $p(u|\underline{x})$ instead is modeled using an explicit distribution. If measurement sources are assumed to be equally distributed on the target's surface, the slice distribution scales linearly with the perimeter of a given slice. Therefore, the slice distribution can be modeled as triangular distribution between 0 and 1 [16]. This triangular distribution can be approximated as normal distribution with $\mathrm{E}\{u\} = \frac{1}{3}$ and $\mathrm{Var}\{u\} = \frac{1}{18}$ by means of moment matching [16]. Finally, an estimator for elliptic cones using extrusion RHMs can be developed using the likelihood

$$p(\underline{y}|\underline{x}) = \int_U \mathcal{N}\left(\underline{y}; c(u, \hat{s}, \underline{p}), \mathbf{C}_w\right) \cdot \mathcal{N}\left(u; \frac{1}{3}, \frac{1}{18}\right) du. \tag{12}$$

An illustration of an extrusion RHM for elliptic cones can be seen in Fig. 4, where the slice distribution is depicted by coloring the shape with red for high probability changing to blue for low probability. For a given slice, the GAM part can be reduced to 2D space by finding the closest point on a slice ellipse $e(u, s, \underline{p})$ to a given measurement $\underline{\tilde{y}}_{x,y} = [\tilde{y}_x, \tilde{y}_y]^T$ which is given as

$$e(u, s, \underline{p}) = \begin{bmatrix} (1-u) \cdot a \cdot \cos(s) \\ (1-u) \cdot b \cdot \sin(s) \end{bmatrix}. \tag{13}$$

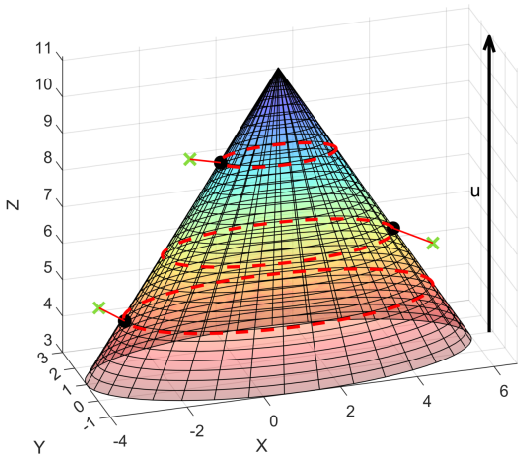

Fig. 4: Illustration of extrusion RHM with the color gradient indicating the distribution of the height parameter u.

For finding the closest point on an ellipse to a given point, we propose to use analytic solutions which can be found, e.g. in [26]. This extrusion RHM for elliptic cones is capable of producing satisfying height estimates due to the explicitly applied slice distribution. Additionally, it is capable of handling partial occlusions by design like the GAM presented before. However, for high noise, estimating the half axes can still be biased because of the applied GAM part in the extrusion RHM. This problem could be solved by integrating a partial information model (PIM) part [16], [24] instead of the GAM part. However, as we aim to process data of a multilayer LiDAR sensor that produces measurements with low measurement noise, the GAM part in the extrusion RHM is sufficient. To produce unbiased height estimates, the distribution of the height parameter must not be approximated with a Gaussian distribution. However, this would mean that the S²KF can no longer be used as it calculates an arbitrary number of samples from a multidimensional Gaussian distribution.

IV. Implementation

In this section, some more insights on implementing the aforementioned models are presented. In this paper, every model is implemented using the S²KF [22] due to its straightforward implementation. Equations for the prediction and update step of the S²KF can be found in [22]. However, other filtering techniques like the progressive Gaussian filter (PGF) [27] for example could also be appropriate. Nonlinear estimators like the PGF could outperform the S²KF, however, an explicit likelihood function is needed [28] which can be hard to calculate due to the integrals in (5) and (6). The kinematic evolution over time is modeled as coordinated turn [23] with constant cone parameters, i.e., the cone dimensions being constant over time. Measurement equations for the update steps are presented in the following.

A. GAM

When implementing a GAM for an elliptic cone, the first step is to calculate the measurement in object local coordinates

as

$$\tilde{\underline{y}} = \mathbf{R}_{\psi}^{-1} \cdot \left(\underline{y} - \underline{m}\right) \tag{14}$$

with 3D rotation matrix $\mathbf{R}_{\psi}$ for the yaw angle (in the xy-plane). The greedy point estimate can now be calculated as the closest point of the measurement in local coordinates to the predicted shape as

$$c(\hat{u}, \hat{s}, \underline{p}) = \min_{s\in[0,2\pi]\,,\, u\in[0,1]} \left(\|\tilde{\underline{y}} - c(u, s, \underline{p})\|_2\right). \tag{15}$$

We propose to use analytic solutions of the minimization problem as outlined in Sec. III-B for computation time reasons. However, numeric solutions can be applied as well. Given the measurement source (15) for an elliptic cone GAM, the final measurement equation is given as

$$\underline{0} = h(\underline{x}, \underline{y}) = \mathbf{R}_{\psi} \cdot c(\hat{u}, \hat{s}, \underline{p}) + \underline{m} - \underline{y}\,, \tag{16}$$

where $\underline{0}$ can be interpreted as a constant pseudo-measurement. Please note that we assume isotropic white zero-mean Gaussian noise, which can be handled inherently by the S²KF. So the system state must not be extended by the measurement noise to sample the joint distribution as was intended in [22]. Instead, the measurement noise covariance matrix can be added to the measurement covariance matrix in the update step.

B. Extrusion RHM

When implementing an extrusion RHM, the GAM part breaks down to 2D space as already mentioned in Sec. III-C. However, the height parameter u has to be sampled for every measurement from the Gaussian distribution $p(u|\underline{x})$, cf. (12). With a given measurement in local coordinates (14) and a sampled parameter u, the greedy point estimate can be calculated as

$$c(u, \hat{s}, \underline{p}) = \begin{bmatrix} \min\limits_{s\in[0,2\pi]} (\|\tilde{\underline{y}}_{x,y} - e(u, s, \underline{p})\|_2) \\ u \cdot h \end{bmatrix}. \tag{17}$$

Again we propose to use analytic solutions [26] for finding the estimate for the closest point on an ellipse. Finally, the measurement equation for an elliptic cone extrusion RHM is

$$\underline{0} = h(\underline{x}, \underline{y}) = \mathbf{R}_{\psi} \cdot c(u, \hat{s}, \underline{p}) + \underline{m} + \underline{w} - \underline{y} \tag{18}$$

with the constant pseudo-measurement $\underline{0}$. Since the parameter u is modeled as multiplicative noise, the height cannot be estimated with a standard linear estimator. Therefore, we suggest to extend the measurement equation to a quadratic estimator as proposed in [15], [22], [29]. The extended measurement equation can then be given as

$$\begin{bmatrix} \underline{0} \\ \underline{0} \end{bmatrix} = \begin{bmatrix} \mathbf{R}_{\psi} \cdot c(u, \hat{s}, \underline{p}) + \underline{m} + \underline{w} - \underline{y} \\ \left(\mathbf{R}_{\psi} \cdot c(u, \hat{s}, \underline{p}) + \underline{m} + \underline{w}\right)^{\circ 2} - (\underline{y})^{\circ 2} \end{bmatrix} \tag{19}$$

using element-wise squaring. Please note that the measurement noise $\underline{w}$ is integrated in the measurement equation (19). This means, that the joint density $f_{X,W,U}(\underline{x}, \underline{w}, \underline{u})$ of the system state extended by the measurement noise $\underline{w}$ and the height parameter u has to be sampled for an update using the S²KF [22].

C. Update step with multiple measurements

As a measurement set $\mathcal{Y}_k$ with n_k measurements is recorded every time step, a procedure for updating the system state using all measurements is needed. A first intuitive way is to process measurements sequentially in multiple update steps. Therefore, the density $f_X(\underline{x})$ for a GAM or the joint density $f_{X,W,U}(\underline{x}, \underline{w}, \underline{u})$ for an extrusion RHM has to be sampled every sequence of update procedures with the latest update. Another possibility is to update the system state $\underline{x}_k$ simultaneously with all measurements $\mathcal{Y}_k$ by aggregating them into a single measurement vector. A measurement update can then be performed by extending the measurement equation using the aggregated measurement vector. Please see [15] for example for more details. A major drawback of RHMs is discernible at this point, since the extended system state has to be sampled. This means, for every measurement $\underline{y}_{k,l}$ the height parameter $u_{k,l}$ and the measurement noise $\underline{w}_{k,l}$ has to be sampled individually. This results in a possibly large system state with a varying number of state variables when performing a single measurement update. Solutions could be to fix the maximum number of measurements processed in the update step and to decide for an optimal measurement set to represent the extent of the target or to simply use a single measurement update for every measurement.

V. Simulation experiments

In this section, both new models are investigated in simulated scenarios. Therefore, a static and a dynamic scenario are considered. In both scenarios, measurements are generated by sampling the parameters s and u and integrating them into the shape function (3). The parameter s is sampled from a uniform distribution $s \sim \mathcal{U}\left(0, \frac{3\pi}{2}\right)$. The parameter u is sampled from a triangular distribution $u \sim \mathcal{T}(0, 0, 1)$ with peak and the lower limit at 0 and the upper limit at 1, thus, the same that is assumed for the extrusion RHM in Sec. III-C. However, only parameters smaller than 0.8 are forced to be sampled. Hence, measurements are drawn from an artificially occluded object to demonstrate the capability of both models to track occluded targets. If an SDM would be used with a uniform distribution on the entire surface, it could not handle this occlusion since the assumption of a uniform distribution would be corrupted. The system state is sampled with 10 samples per dimension in each simulation experiment using the routine of the S²KF [22], [30].

A. Static scenario

In the static scenario, 1500 measurements are drawn for a single simulation run and corrupted by isotropic noise with a standard deviation of $\sigma_w = 0.05\,\mathrm{m}$. In every simulation run, the position and orientation of the elliptic cone are initialized with the reference as the experiment is intended to mainly investigate the extent estimation of both models. In this simulation, the measurement noise is low as would be with a multilayer LiDAR sensor to show the capability of both models to estimate the extent of the target. The reference cone is implemented with parameters $a = 5\,\mathrm{m}$ for major half axis,

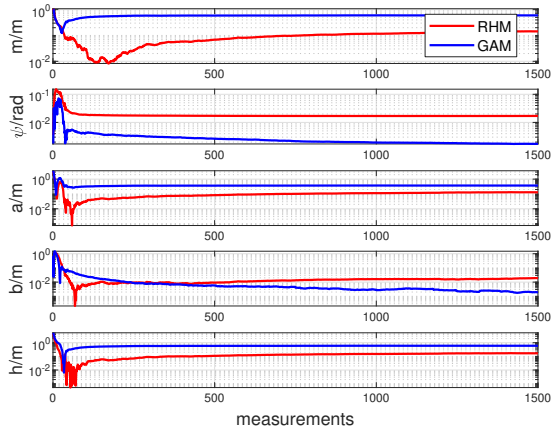

Fig. 5: RMSEs of static scenario.

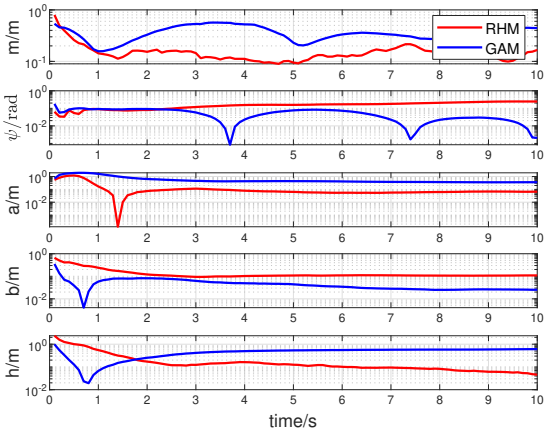

Fig. 6: RMSEs of dynamic scenario.

$b = 2\,\text{m}$ for minor half axis and height $h = 8\,\text{m}$. The system state is initialized with position $\underline{m} = [1, 1, 3]^T$, orientation $\psi = 0.3\,\text{rad}$ and shape $\underline{p} = [1, 1, 1]^T$. The system state covariance matrix is initialized as $P = \text{diag}(1, 1, 1, 1, 5, 5, 5)$. In the static simulation, the prediction step is completely neglected. In Fig. 5, root mean square errors (RMSEs) of a Monte Carlo simulation with 100 runs are depicted. It is evident that the height of the cone is estimated better when using an extrusion RHM instead of a GAM. This performance gain can be attributed to the correctly assumed distribution in the height parameter which directly affects the estimation accuracy of any other state parameter in the static scenario. Finally, it ensures better performance of the extrusion RHM compared to the GAM. The better height estimate of the GAM can be affiliated with the inability of GAMs to penalize overestimated lengths. For more details, see [25, p. 74].

B. Dynamic scenario

In the dynamic scenario, a single reference trajectory was generated using a coordinated turn model [23] in 2D space corrupted by noise with $\sigma_{v_{xy}} = 2.2\,\text{m/s}^2$ for polar velocity and $\sigma_{\dot{\psi}} = 1.5\,°/\text{s}^2$ for turn rate. The z-component of the position is modeled to be constant. The sampling rate is simulated as $dt = 0.1\,\text{s}$. Every time step, 15 measurements are drawn and corrupted by isotropic measurement noise with $\sigma_w = 0.3\,\text{m}$. In this simulation, higher measurement noise is chosen to show the capability of the models to track the target even with high measurement noise. In the prediction step, the same coordinated turn model with the same system uncertainties is used with a constant z-component in the position and constant cone parameters. The cone parameters of the reference are chosen to be the same as in the static scenario. In this simulation, the system state is initialized using the first measurement set. The position in the xy-plane is taken to be the mean position

$$\underline{m}_{xy} = \frac{1}{15}\left(\sum_{i=1}^{15} \underline{y}_{xy}^{(i)}\right) \tag{20}$$

of the first measurement set. The z-position is initialized as the minimum z-value. In the following, the covariance matrix

$$\mathbf{C}_m = \text{Cov}\left(y_x^{(i)}, y_y^{(i)}\right) \quad i = 1, \ldots, 15 \tag{21}$$

of the first measurement set is calculated. The orientation of the covariance matrix $\mathbf{C}_m$ is used as initialization for the system state. The parameters a and b are taken to be twice the major and minor eigenvalues of the covariance matrix $\mathbf{C}_m$, respectively. Finally, the height is initialized as the distance between the maximum and minimum z-components of the first measurement set. The covariance of the system state is set to be $\mathbf{C}_m$ for position in xy-plane, 1 for other described parameters and 5 for velocity components that are initialized to be 0.

In Fig. 6, again RMSEs of a Monte Carlo simulation with 100 runs are depicted. In this simulation, the improvement of the estimation outcome when using an extrusion RHM compared to the GAM is as clear as before in the static scenario. The height estimate converges to the true value when using an extrusion RHM. The height estimate of the GAM is biased as expected. Thus, the position estimate of the extrusion RHM outperforms the GAM as well. However, the extrusion RHM is still biased in the estimation of the half axes a and b because of the GAM part for the parameter s. As a consequence, the GAM even outperforms the extrusion RHM in the estimation of the half axis b.

VI. Real Data Experiments

In this section, 3D measurements of a sailing boat as can be seen in Fig. 1 are fused to estimate the extent of the sailing boat approximated as an elliptic cone. The measurements were taken by a ferry on Lake Constance that had to go through a regatta of folk boats. These folk boats are standardized with a length of 7.68 m, a width of 2.2 m, and a mast height over the water surface of 9.95 m which serves as a reference for our extent estimation experiments [31].

The measurements were recorded from an Alpha Prime multilayer LiDAR sensor [32]. This sensor has a 360° horizontal and 40° vertical field of view. The measurement range is up

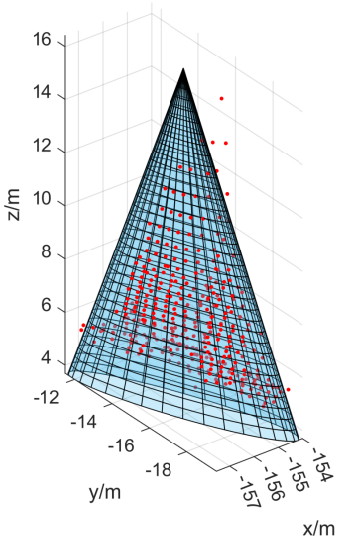

Fig. 7: Extension estimation using a GAM.

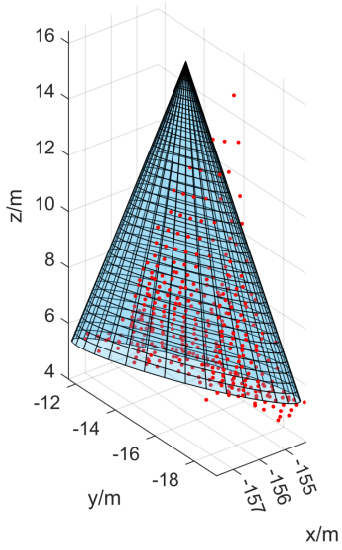

Fig. 8: Extension estimation using an extrusion RHM.

to 245 m, the sensor has 128 channels and measurements are recorded with a variable frame rate of 5 Hz to 20 Hz. In this paper, measurements are taken with a frame rate of 10 Hz. The sensor has a minimum angular vertical resolution of $0.11°$ and an angular horizontal resolution between $0.1°$ and $0.4°$ depending on the frame rate.

As measurement model, a coordinated turn model [23] is used in the xy-plane like in the simulated dynamic scenario before. Additionally, a constant velocity movement is added in z-direction to allow the object to change the position in z. The system uncertainties are taken to be $\sigma_{v_{xy}} = 1\,\text{m/s}^2$ for velocity in the xy-plane, $\sigma_{\dot{\psi}} = 1\,°/\text{s}^2$ for the turn rate and $\sigma_{v_z} = 0.05\,\text{m/s}^2$ for the velocity in z-direction. Additionally, uncertainties of $\sigma_a = \sigma_b = \sigma_h = 10^{-3}\,\text{m}$ are assumed for the cone parameters in order to prevent local minima during the estimation procedure. The initialization scheme of the system state is taken from Sec. V-B. The system covariance matrix is initialized with $\mathbf{C}_m$ for the position in the xy-plane, 3 m for the position in z-direction, 1 m/s for the velocity in z-direction, 3 m/s for the velocity in the xy-plane, $30°$ for the heading angle, $5\,°/\text{s}$ for the turn rate and 1 m for every cone parameter.

When performing the estimation procedure, we found out that the distribution of the height parameter u does not follow an exact triangular distribution as described in Sec. V. Therefore, we transformed all recorded measurements of the whole scenario to a local coordinate system and calculated the statistical mean and variance of the height parameter u and approximated it as Gaussian distribution

$$p(u|\underline{x}) = \mathcal{N}\left(u; 0.2902, 0.0434\right). \tag{22}$$

In Fig. 7 and Fig. 8 estimation results applying an elliptic cone GAM and extrusion RHM respectively to measurements of a sailing boat in a single time step are depicted. The z-position is estimated more accurately when using an extrusion RHM and estimated too low for a GAM. This causes the height and length to be overestimated as well when using a GAM. In the figures, it can also be seen, that the peak of the cone does not fit the maximum measurement of the sailing boat. This is caused by the fact that the mast is not centered on the boat hull to be assumed a regular elliptic cone. In Fig. 9, estimated cone parameters for the whole scenario are depicted as well as the parameters of a folk boat as described before. It turns out that the suspicion of an overestimated height and length parameter is correct when using a GAM. In comparison, length is estimated quite accurately when using an extrusion RHM. The height estimate of the extrusion RHM is slightly overestimated, indeed better in comparison to the GAM. The width of the boat is underestimated by both models which could be caused by the GAM part in both models or the not perfectly fitting shape approximation.

VII. Conclusion and Future Work

In this paper, we presented a new 3D shape approximation for sailing boats. Thus, we proposed two different models to solve the measurement source association problem, namely a GAM and an extrusion RHM for elliptic cones. We investigated both models in a simulated static and dynamic scenario, as well as in a real-world scenario recorded by an Alpha Prime mounted on a ferry on Lake Constance. Simulations and the real-world scenario showed that both models were capable of tracking the extent of the target. We saw, that the height estimate is more stable when using an actual distribution for the height parameter that fits the measurements. However, unbiased height estimates would require sampling from a mixed Gaussian and triangular distribution. Finally, we saw that both models are capable of estimating the extent of the target and tracking the sailing boat.

In future work, the parameters of the Gaussian defining the distribution of the height parameter could be set adaptively

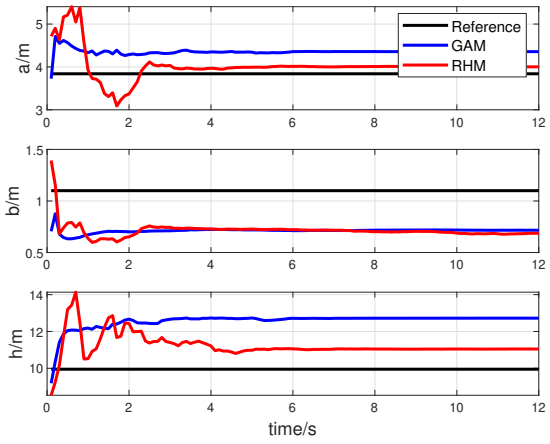

Fig. 9: Results of parameter estimation applying GAM and extrusion RHM.

and learned from actual data. Also, the shape itself could be slightly adapted by adding a shear transform or shifting the center and peak of the cone to better fit the position of the mast. Finally, mixed Gaussian and triangular sampling of the mixed joint density could be investigated or other appropriate filters like the PGF [27] could be used to produce better estimation results.

REFERENCES

[1] K. Granström, M. Baum, and S. Reuter, "Extended object tracking: Introduction, overview, and applications," *Journal of Advances in Information Fusion*, vol. 12, Dec. 2017.

[2] M. Feldmann, D. Fränken, and W. Koch, "Tracking of extended objects and group targets using random matrices," *IEEE Transactions on Signal Processing*, vol. 59, no. 4, pp. 1409–1420, 2011.

[3] M. Baum, B. Noack, and U. D. Hanebeck, "Extended object and group tracking with elliptic random hypersurface models," in *13th International Conference on Information Fusion (FUSION)*, 2010, pp. 1–8.

[4] K. Thormann, S. Yang, and M. Baum, "A comparison of Kalman filter-based approaches for elliptic extended object tracking," in *IEEE 23rd International Conference on Information Fusion (FUSION)*, 2020, pp. 1–8.

[5] K. Thormann and M. Baum, "Fusion of elliptical extended object estimates parameterized with orientation and axes lengths," *IEEE Transactions on Aerospace and Electronic Systems*, vol. 57, no. 4, pp. 2369–2382, 2021.

[6] K. Granström, C. Lundquist, and U. Orguner, "Tracking rectangular and elliptical extended targets using laser measurements," in *14th International Conference on Information Fusion (FUSION)*, 2011.

[7] P. Broßeit, M. Rapp, N. Appenrodt, and J. Dickmann, "Probabilistic rectangular-shape estimation for extended object tracking," in *IEEE Intelligent Vehicles Symposium (IV)*, 2016, pp. 279–285.

[8] H. Kaulbersch, J. Honer, and M. Baum, "A Cartesian B-spline vehicle model for extended object tracking," in *21st International Conference on Information Fusion (FUSION)*, 2018.

[9] A. Scheel and K. Dietmayer, "Tracking multiple vehicles using a variational radar model," *IEEE Transactions on Intelligent Transportation Systems*, vol. 20, no. 10, pp. 3721–3736, 2019.

[10] J. Honer and H. Kaulbersch, "Bayesian extended target tracking with automotive radar using learned spatial distribution models," in *2020 IEEE International Conference on Multisensor Fusion and Integration for Intelligent Systems (MFI)*, 2020, pp. 316–322.

[11] H. Kaulbersch, J. Honer, and M. Baum, "EM-based extended target tracking with automotive radar using learned spatial distribution models," in *2019 22th International Conference on Information Fusion (FUSION)*, 2019, pp. 1–8.

[12] M. Baum and U. D. Hanebeck, "Shape tracking of extended objects and group targets with star-convex RHMs," in *14th International Conference on Information Fusion (FUSION)*, 2011.

[13] N. Wahlström and E. Özkan, "Extended target tracking using Gaussian processes," *IEEE Transactions on Signal Processing*, vol. 63, no. 16, pp. 4165–4178, 2015.

[14] K. Thormann, M. Baum, and J. Honer, "Extended target tracking using Gaussian processes with high-resolution automotive radar," in *2018 21st International Conference on Information Fusion (FUSION)*, 2018, pp. 1764–1770.

[15] F. Faion, M. Baum, and U. D. Hanebeck, "Tracking 3D shapes in noisy point clouds with random hypersurface models," in *15th International Conference on Information Fusion (FUSION)*, 2012, pp. 2230–2235.

[16] F. Faion, A. Zea, J. Steinbring, M. Baum, and U. D. Hanebeck, "Recursive Bayesian pose and shape estimation of 3D objects using transformed plane curves," in *Sensor Data Fusion: Trends, Solutions, Applications (SDF)*, 2015.

[17] A. Zea, F. Faion, and U. D. Hanebeck, "Tracking extended objects using extrusion random hypersurface models," in *Sensor Data Fusion: Trends, Solutions, Applications (SDF)*, 2014.

[18] G. Kurz, F. Faion, F. Pfaff, A. Zea, and U. D. Hanebeck, "Three-dimensional simultaneous shape and pose estimation for extended objects using spherical harmonics," 2020.

[19] T. Baur, J. Reuter, A. Zea, and U. D. Hanebeck, "Shape estimation and tracking using spherical double Fourier series for three-dimensional range sensors," in *2021 IEEE International Conference on Multisensor Fusion and Integration for Intelligent Systems (MFI)*, 2021, pp. 1–6.

[20] M. Kumru and E. Özkan, "Three-dimensional extended object tracking and shape learning using Gaussian processes," *IEEE Transactions on Aerospace and Electronic Systems*, vol. 57, no. 5, pp. 2795–2814, 2021.

[21] M. Schuster, J. Reuter, and G. Wanielik, "Multi detection joint integrated probabilistic data association using random matrices with applications to radar-based multi object tracking," *Journal of Advances in Information Fusion*, vol. 12, no. 2, pp. 175 – 188, 2017.

[22] J. Steinbring and U. D. Hanebeck, "S2KF: The smart sampling Kalman filter," in *Proceedings of the 16th International Conference on Information Fusion (FUSION)*, 2013, pp. 2089–2096.

[23] M. Roth, G. Hendeby, and F. Gustafsson, "EKF/UKF maneuvering target tracking using coordinated turn models with polar/Cartesian velocity," in *17th International Conference on Information Fusion (FUSION)*, 2014.

[24] F. Faion, A. Zea, M. Baum, and U. D. Hanebeck, "Partial likelihood for unbiased extended object tracking," in *18th International Conference on Information Fusion (FUSION)*, 2015, pp. 1022–1029.

[25] F. Faion, "Tracking extended objects in noisy point clouds with application in telepresence systems," Ph.D. dissertation, Karlsruher Institut für Technologie (KIT), 2016.

[26] A. Y. Uteshev and M. V. Goncharova, "Point-to-ellipse and point-to-ellipsoid distance equation analysis," *Journal of Computational and Applied Mathematics*, vol. 328, pp. 232–251, 2018.

[27] J. Steinbring and U. D. Hanebeck, "Progressive Gaussian filtering using explicit likelihoods," in *17th International Conference on Information Fusion (FUSION)*, 2014, pp. 1–8.

[28] J. Steinbring, M. Baum, A. Zea, F. Faion, and U. D. Hanebeck, "A closed-form likelihood for particle filters to track extended objects with star-convex RHMs," in *2015 IEEE International Conference on Multisensor Fusion and Integration for Intelligent Systems (MFI)*, 2015, pp. 25–30.

[29] M. Baum, F. Faion, and U. D. Hanebeck, "Modeling the target extent with multiplicative noise," in *2012 15th International Conference on Information Fusion (FUSION)*, 2012, pp. 2406–2412.

[30] J. Steinbring, "Nonlinear estimation toolbox." [Online]. Available: https://bitbucket.org/nonlinearestimation/toolbox

[31] *Revision of the Class Regulations and the Class Racing Regulations*, Folkboat Assn, February 2012, Rev. 2012.

[32] *Alpha Prime Powering Safe Autonomy*, Velodyne Lidar, 2019, Rev. 1.